Enhancing the Bandwidth of Gravitational-Wave Detectors with Unstable Optomechanical Filters

Haixing Miao,[1] Yiqiu Ma,[2] Chunnong Zhao,[2] and Yanbei Chen[3]
[1]School of Physics and Astronomy, University of Birmingham, Birmingham B15 2TT, United Kingdom
[2]School of Physics, University of Western Australia, Western Australia 6009, Australia
[3]Theoretical Astrophysics 350-17, California Institute of Technology, Pasadena, California 91125, USA
(Received 18 June 2015; revised manuscript received 29 September 2015; published 17 November 2015)

Advanced interferometric gravitational-wave detectors use optical cavities to resonantly enhance their shot-noise-limited sensitivity. Because of positive dispersion of these cavities—signals at different frequencies pick up different phases, there is a tradeoff between the detector bandwidth and peak sensitivity, which is a universal feature for quantum measurement devices having resonant cavities. We consider embedding an active unstable filter inside the interferometer to compensate the phase, and using feedback control to stabilize the entire system. We show that this scheme in principle can enhance the bandwidth without sacrificing the peak sensitivity. However, the unstable filter under our current consideration is a cavity-assisted optomechanical device operating in the instability regime, and the thermal fluctuation of the mechanical oscillator puts a very stringent requirement on the environmental temperature and the mechanical quality factor.

DOI: 10.1103/PhysRevLett.115.211104 PACS numbers: 04.80.Nn, 03.65.Ta, 42.50.Lc, 07.10.Cm

Introduction.—Current ground-based gravitational-wave (GW) detectors, including Advanced LIGO [1], Advanced VIRGO [2], and KAGRA [3], are kilometer-scale laser interferometers that measure GW-induced differential arm length change. These detectors are macroscopic in size, and yet one of the major noises that limit their sensitivity is the quantum noise—quantum radiation pressure noise at low frequencies and quantum shot noise at high frequencies (above ~100 Hz). To reduce the shot noise, they incorporate optical cavities in two arms that resonantly enhance both the optical power and signal, as shown schematically in Fig. 1(a). In addition, they include a power-recycling mirror (PRM) at the bright (common) port and a signal-recycling mirror (SRM) at the dark (differential) port—PRM further increases the power circulating inside arm cavities, e.g., up to ~1 MW for Advanced LIGO, while SRM coherently reflects the signal back to the interferometer and modifies the detector response to GW signals at different frequencies. For instance, Advanced LIGO, in its nominal operation mode, uses a SRM to broaden the detector bandwidth, which equalizes the response to both low-frequency and high-frequency signals. However, this is at a price of decreasing the peak sensitivity when considering the shot noise, as illustrated in Fig. 1(b). Such a tradeoff between the bandwidth and the peak sensitivity (with their product being approximately constant) can be attributable to the positive dispersion of optical cavities—signals at different frequencies are not simultaneously resonant due to the frequency-dependent propagation phase. This feature was first pointed out by Mizuno [4] in the GW community. It turns out to be universal for all quantum measurement devices with resonant cavities, e.g., optomechanically based force or position sensors [5], and laser ring gyros [6]. The bandwidth-sensitivity product is ultimately bounded by the amount of energy stored inside the devices, which is a consequence of the quantum Cramér-Rao bound [7,8].

There are several approaches proposed in the literature aiming at increasing the bandwidth-sensitivity product. They generally fall into two categories: (i) a sensitivity-oriented category—using external squeezing [9,10] or internal squeezing [11,12] to reduce the shot noise while keeping broad bandwidth (external squeezing has been implemented in large-scale GW detectors [13,14] and is also planned for future upgrades [15–17]), and (ii) a bandwidth-oriented category—the so-called white-light-cavity idea [18–25]—that uses an atomic medium with negative dispersion to cancel the positive dispersion of optical cavities.

We consider a different approach to improve the broadband-sensitivity product by embedding an unstable filter inside the interferometer to compensate the phase, and the

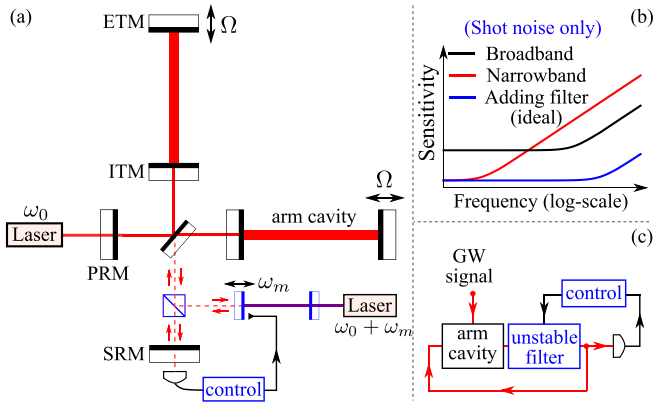

FIG. 1 (color online). (a) The typical laser interferometer configuration for advanced GW detectors, with an unstable optomechanical filter (blue) embedded. (b) The tradeoff between the detector bandwidth and peak sensitivity (black and red curves), and the effect of adding an unstable filter in the ideal scenario (blue). (c) A simple flow chart for the entire scheme.

entire scheme is stabilized via feedback control. Notice that different from the stable atomic medium proposed previously, such a filter is not constrained by the Kramers-Kronig relation, and yet there is no violation of causality, as the controlled system is stable and the measured output always lags behind incoming GW signals. In addition, as indicated by the flow chart in Fig. 1(c), the feedback uses output that contains both the signal and noise, and therefore it does not influence the signal-to-noise ratio, as proven in Refs. [26,27]. One realization of the unstable filter that we consider here is an optomechanical device operating in the instability regime pumped by an additional laser, as illustrated schematically in Fig. 1(a). This is inspired by recent experimental observations of the optomechanical analogue of the electromagnetically induced transparency by Weis *et al.* [28], Teufel *et al.* [29], and Safavi-Naeini *et al.* [30], and also a more recent theoretical proposal by Ma *et al.* [31].

A brief summary.—Before delving into the details, we summarize the main features and explain them qualitatively. For the main interferometer, arm cavities are tuned to be resonant with respect to the input laser (carrier light) at frequency ω_0, i.e., $\omega_0 L_{\rm arm}/c = N\pi$ with $L_{\rm arm}$ the arm cavity length (4 km for Advanced LIGO) and N an integer. GW-induced motion of the end test masses (ETMs) modulates the carrier and creates signal sidebands at $\omega_0 + \Omega$ with Ω being the GW frequencies. When propagating inside the arm cavity, these sidebands pick up the extra phase of $\phi_{\rm arm}(\Omega) = 2\Omega L_{\rm arm}/c$ (round-trip) compared with the carrier. In order to make these sidebands also resonant inside the arm cavities, ideally we need to insert an optical filter with negative dispersion to cancel such an extra phase: $\phi_{\rm arm}(\Omega) + \phi_{\rm filter}(\Omega) = 0$, namely,

$$\phi_{\rm filter}(\Omega)|_{\rm ideal\ case} = -2\Omega L_{\rm arm}/c. \tag{1}$$

In addition, the filter should not distort the GW waveform, or equivalently, the modulus of its frequency-domain transfer function needs to be close to unity—an all-pass filter. Because of the famous Kramers-Kronig relation, any stable filter can only approximate such a negative-dispersion all-pass filter within a certain frequency band. In contrast, this is no longer a constraint for unstable filters, if one can find a realistic realization and proper feedback control scheme—the unstable optomechanical filter presented here provides such an example.

Specifically, for the optomechanical filter, the radiation pressure couples the optical field intensity and the mechanical displacement. Such a nonlinear coupling is analogous to the three-wave mixing in nonlinear optics. By tuning the pump laser frequency to be $\omega_0 + \omega_m$ with the mechanical oscillator frequency ω_m much larger than the cavity bandwidth γ_f, i.e., the so-called resolved-sideband regime $\omega_m \gg \gamma_f \gg \Omega$, the cavity resonance at ω_0 is in favor of the down-conversion process, which amplifies the sidebands around ω_0 and mechanical motion. It can be viewed as a phase-insensitive parametric amplifier for sidebands with the following input-output relation:

$$\hat{a}_{\rm out}(\Omega) \approx \frac{\Omega + i(\gamma_m + \gamma_{\rm opt})}{\Omega + i(\gamma_m - \gamma_{\rm opt})}\hat{a}_{\rm in}(\Omega). \tag{2}$$

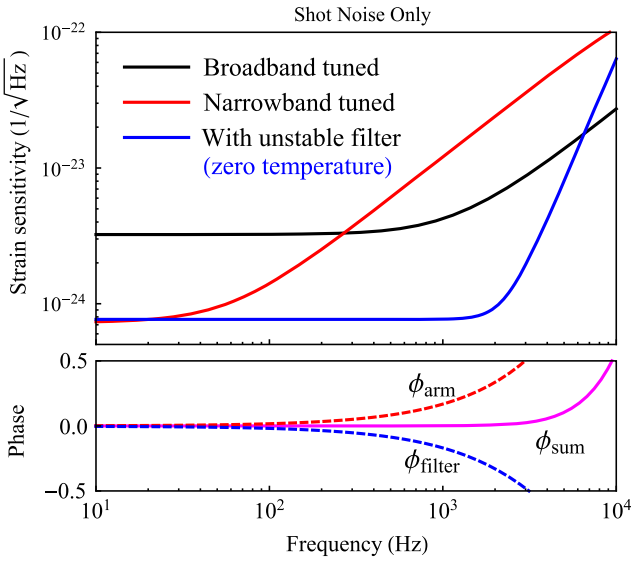

FIG. 2 (color online). The top panel shows the shot-noise-only strain sensitivity of the unstable-filter scheme, compared with the broadband and narrow-band tuned cases without the filter. The power and arm cavity length are the same as for Advanced LIGO. At high frequencies, the sensitivity deviates from the ideal scenario, because of imperfect phase cancellation of higher-order terms of Ω in $e^{i\phi_{\rm arm}(\Omega)}$ (bottom panel).

Here, $\gamma_m \equiv \omega_m/Q_m$ is the mechanical damping rate with Q_m being the quality factor; $\gamma_{\rm opt}$ is the negative mechanical damping rate due to the optomechanical interaction, and is approximately equal to $P_c\mathcal{F}\omega_0/(m\omega_m c^2)$, where P_c is the intracavity laser power, $\mathcal{F}$ is the cavity finesse, and m is the mass of the mechanical oscillator.

The unstable regime we referred to is when $\gamma_{\rm opt}$ becomes much larger than γ_m and the mechanical damping rate becomes negative. With the feedback control engaged, the open-loop input-output relation of the optomechanical filter is

$$\hat{a}_{\rm out}(\Omega) \approx \frac{\Omega + i\gamma_{\rm opt}}{\Omega - i\gamma_{\rm opt}}\hat{a}_{\rm in}(\Omega) \approx -\exp\left(-\frac{2i\Omega}{\gamma_{\rm opt}}\right)\hat{a}_{\rm in}(\Omega). \tag{3}$$

This realizes the all-pass filter with phase in Eq. (1) when

$$\gamma_{\rm opt} = c/L_{\rm arm}, \tag{4}$$

and the resulting intracavity laser power of the filter scales as

$$P_c \approx 10^2 W\left(\frac{4\ {\rm km}}{L_{\rm arm}}\right)\left(\frac{10\ {\rm MHz}}{\omega_m/2\pi}\right)\left(\frac{0.1{\rm mg}}{m}\right)\left(\frac{\mathcal{F}}{10^5}\right). \tag{5}$$

In Fig. 2, we show the corresponding shot-noise-only sensitivity with the nominal parameters given above and one additional parameter $L_f = 1$ cm being the filter cavity length. We can see that the unstable filter can compensate the phase at low frequencies but is not perfect at high frequencies due to the high-order frequency dependence of the phase delay, which in principle can be improved by cascading several unstable filters.

So far, we have only mentioned the phase property of the unstable filter. As a general principle proven by Caves for

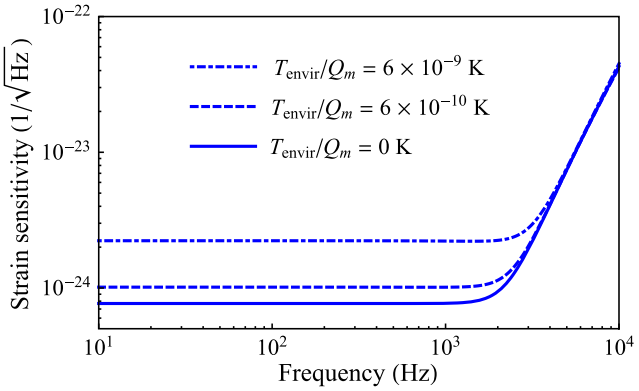

FIG. 3 (color online). Effect of the thermal fluctuation of the mechanical oscillator on the sensitivity.

phase-insensitivity parametric amplifiers [32], there will be an additional noise term given Eq. (2). As shown later, it comes from the thermal noise of the mechanical oscillator. In order for its effect not to be significant, we require

$$8k_B T_{\rm envir}/Q_m \lesssim \hbar\gamma_{\rm IFO}, \tag{6}$$

where k_B is the Boltzmann constant, $T_{\rm envir}$ is the environmental temperature, and $\gamma_{\rm IFO}$ is the original detector bandwidth before introducing the unstable filter. Therefore, the lower the detector bandwidth is that we start off with, the higher is the requirement that will be imposed on the temperature and quality factor. As an order of magnitude estimation, we have

$$\frac{T_{\rm envir}}{Q_m} \lesssim 6 \times 10^{-10}\ {\rm K}\left(\frac{\gamma_{\rm IFO}/2\pi}{100\ {\rm Hz}}\right). \tag{7}$$

In Fig. 3, we show the thermal noise effect on the sensitivity. As mentioned in Ref. [31], one approach for mitigating such a thermal-noise effect is applying the optical-dilution idea [33–36], which uses optically induced rigidity to dilute the mechanical dissipation, and allows for enhancement of Q_m by a factor of 100 or even more, but further experimental study is necessary. After this summary, we will present more details about the scheme and also the issue of feedback control.

Dynamics of the optomechanical filter.—We start with the optomechanical filter shown in Fig. 4(a), derive the input-output relation for the sidebands, and later combine it with the main interferometer. It is an optomechanical device that has been studied extensively in the literature (see the recent reviews in Refs. [5,37]), with the Hamiltonian given by $\hat{H}_{\rm filter} = \hat{H}_0 + \hat{H}_{\rm int} + \hat{H}_{\gamma_f} + \hat{H}_{\gamma_m}$. The free part $\hat{H}_0$ is

$$\hat{H}_0 = \hbar\omega_0 \hat{a}^\dagger \hat{a} + \frac{\hat{p}^2}{2m} + \frac{1}{2} m\omega_m^2 \hat{x}^2. \tag{8}$$

The linearized interaction Hamiltonian $\hat{H}_{\rm int}$ is

$$\hat{H}_{\rm int} = -\hbar g_0 [\hat{a} e^{i(\omega_0+\omega_m)t} + \hat{a}^\dagger e^{-i(\omega_0+\omega_m)t}]\hat{x} \tag{9}$$

with $g_0 \equiv \omega_0 \bar{a}/L_f$ and $\bar{a} = [2P_c L_f/(\hbar\omega_0 c)]^{1/2}$. $\hat{H}_{\gamma_f}$ describes how the cavity mode $\hat{a}$ interacts with the ingoing (outgoing) field $\hat{a}_{\rm in}$ ($\hat{a}_{\rm out}$); $\hat{H}_{\gamma_m}$ describes the coupling between the mechanical oscillator with the environmental thermal bath $\hat{b}_{\rm th}$.

The parameter regime we are interested in, as mentioned earlier, is the so-called resolved-sideband regime illustrated in Fig. 4(b). This allows us to ignore the upper mechanical sideband around $\omega_0 + 2\omega_m$ and use the rotating-wave approximation (RWA) in the interaction picture, obtaining

$$\hat{H}_{\rm int}^{\rm RWA} = -\hbar g(\hat{a}\,\hat{b} + \hat{a}^\dagger \hat{b}^\dagger), \tag{10}$$

where we have introduced the annihilation operator $\hat{b}$ for the mechanical oscillator through $\hat{x}(t) \equiv x_q(\hat{b}e^{-i\omega_m t} + \hat{b}^\dagger e^{i\omega_m t})$ and $g \equiv g_0 x_q$ with x_q being the ground-state uncertainty.

The resulting Heisenberg equations of motion read

$$\dot{\hat{a}}(t) + \gamma_f \hat{a}(t) = ig\hat{b}^\dagger(t) + \sqrt{2\gamma_f}\hat{a}_{\rm in}(t), \tag{11}$$

$$\dot{\hat{b}}(t) + \gamma_m \hat{b}(t) = ig\hat{a}^\dagger(t) + \sqrt{2\gamma_m}\hat{b}_{\rm th}(t). \tag{12}$$

Solving them in the frequency domain, we obtain the input-output relation for sidebands using $\hat{a}_{\rm out} = -\hat{a}_{\rm in} + \sqrt{2\gamma_f}\hat{a}$:

$$\hat{a}_{\rm out} \approx \frac{\Omega + i(\gamma_m + \gamma_{\rm opt})}{\Omega + i(\gamma_m - \gamma_{\rm opt})}\hat{a}_{\rm in} + \frac{2\sqrt{\gamma_m\gamma_{\rm opt}}}{\Omega + i(\gamma_m - \gamma_{\rm opt})}\hat{b}_{\rm th}^\dagger, \tag{13}$$

where we have used $\gamma_f \gg \Omega$ and defined $\gamma_{\rm opt} \equiv g^2/\gamma_f \approx P_c \mathcal{F}\omega_0/(m\omega_m c^2)$. The first term gives Eq. (2) and in Fig. 5, we compare it with the exact phase of the optomechanical filter without the RWA and $\gamma_f \gg \Omega$. The second term is the additional the thermal noise term mentioned earlier, and the spectral density for $\hat{b}_{\rm th}$ is approximately given by $2k_B T_{\rm envir}/(\hbar\omega_m) + 1$.

For the mechanical sideband, the resulting susceptibility is

$$\chi_m(\Omega) = -(i\Omega + \gamma_m - \gamma_{\rm opt})^{-1}. \tag{14}$$

The mechanical motion is unstable in the parameter regime of interest with $\gamma_{\rm opt}$ much larger than the bare mechanical damping rate γ_m, and a feedback control is thus needed. We show the control scheme after considering the filter together with the main interferometer, as given below.

Dynamics of the entire system.—The total Hamiltonian reads $\hat{H}_{\rm tot} = \hat{H}_{\rm IFO} + \hat{H}_{\rm filter} + \hat{H}_{\rm IFO\text{-}filter}$. We can model the main interferometer also as an optomechanical device [38]:

$$\hat{H}_{\rm IFO} = \hbar\omega_0 \hat{d}^\dagger \hat{d} + \hat{H}_{\gamma_{\rm IFO}} + \frac{\hat{P}^2}{2M} - \hbar G_0(\hat{d} + \hat{d}^\dagger)\hat{X} + \hat{X}F_{\rm GW}. \tag{15}$$

Here, $\hat{d}$ is the differential optical mode—a single-mode approximation that is valid when considering a sideband

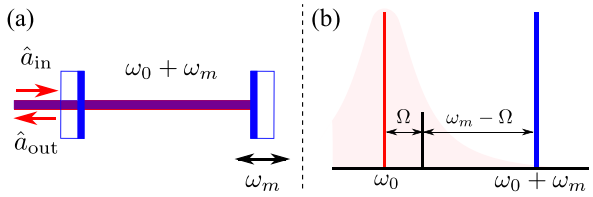

FIG. 4 (color online). (a) Schematics of the optomechanical filter. (b) Frequencies of interest: cavity resonance ω_0 (red), laser frequency $\omega_0 + \omega_m$ (blue), and its lower sideband (black), with the upper sideband around $\omega_0 + 2\omega_m$ (not shown).

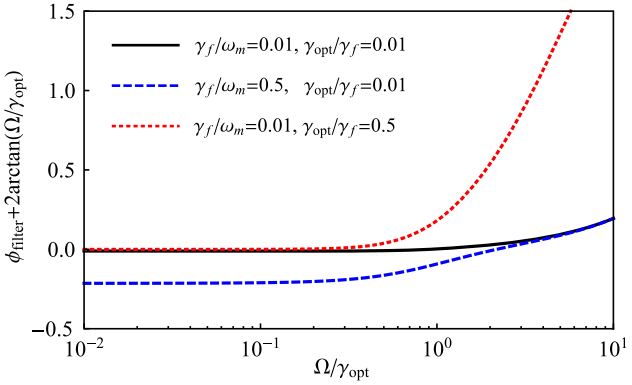

FIG. 5 (color online). The difference between $\phi_{\rm filter}$ obtained without using the RWA and $-2\arctan(\Omega/\gamma_{\rm opt})$. The parameter regime with $\omega_m \gg \gamma_f \gg \gamma_{\rm opt}$ is thus preferred for matching the required frequency dependence.

frequency much lower than one free spectral range $c/(2L_{\rm arm})$, $\hat{H}_{\gamma_{\rm IFO}}$ describes the interaction between $\hat{d}$ and the ingoing (outgoing) field $\hat{a}_{\rm in}(\hat{a}_{\rm out})$ at the dark port, $G_0 = \omega_0 \bar{d}/L_{\rm arm}$ is the coupling strength and $\bar{d} = [2P_{\rm arm}L_{\rm arm}/(\hbar\omega_0 c)]^{1/2}$ with $P_{\rm arm}$ being the arm cavity power, $\hat{X}$ is the differential motion of the ETMs and is driven by the GW as a tidal force, and $F_{\rm GW} = ML_{\rm arm}\ddot{h}(t)$ with h being the GW strain. The coupling between $\hat{d}$ and $\hat{a}$ can be quantified by (exchanging photons)

$$\hat{H}_{\text{IFO-filter}} = \hbar\omega_s(\hat{d}^\dagger\hat{a} + \hat{d}\hat{a}^\dagger), \tag{16}$$

where $\omega_s \equiv \sqrt{c\gamma_f/L_{\rm arm}}$ is the coupling rate, equal to the optomechanical coupling rate g when Eq. (4) is satisfied.

To focus on the shot noise, we will first ignore the radiation pressure effect on the ETMs by assuming $M \to \infty$ (a finite test mass is considered in the rigorous treatment). The resulting equations of motion under the RWA are

$$\dot{\hat{a}} = -i\omega_s\hat{d} + ig\hat{b}^\dagger, \tag{17}$$

$$\dot{\hat{b}}^\dagger = -\gamma_m\hat{b}^\dagger - ig\hat{a} + \sqrt{2\gamma_m}\hat{b}^\dagger_{\rm th}, \tag{18}$$

$$\dot{\hat{d}} = -\gamma_{\rm IFO}\hat{d} - i\omega_s\hat{a} + \sqrt{2\gamma_{\rm IFO}}\hat{d}_{\rm in} + iG_0L_{\rm arm}h. \tag{19}$$

The input-output relation at the SRM is $\hat{d}_{\rm out} = \hat{d}_{\rm in} - \sqrt{2\gamma_{\rm IFO}}\hat{d}$.

The system stability can be examined from the eigenvalues of the dynamical matrix (read off the equations of motion):

$$\mathbf{A} = \begin{bmatrix} 0 & ig & -i\omega_s \\ -ig & -\gamma_m & 0 \\ -i\omega_s & 0 & -\gamma_{\rm IFO} \end{bmatrix}. \tag{20}$$

Having eigenvalues with a positive real part implies instability, which is the case given the relevant parameter regime.

To find the stabilizing controller, we follow the state-space approach. We first need to examine the observability and controllability of the system. It turns out that if we detect the output phase quadrature, which contains the GW signal, using homodyne detection, only one of the two mechanical quadratures will be observed, and this will lead to an uncontrollable system. An apparent solution is measuring both the amplitude and phase quadratures with heterodyne detection. However, this is at a price of increasing the shot noise by $\sqrt{2}$ in amplitude [39]. Instead, we can pick off a small portion of the output signal and use the heterodyne detection only for the control purpose. The rest is still measured using the homodyne detection for extracting the GW signal. As long as we optimally combine it with the pick-off signal using a Wiener filter, the sensitivity will not degrade by a noticeable amount.

In the sideband picture, the resulting readout vector with (using) heterodyne detection is $\mathbf{D} = (0, 0, 1)$—the measured $\hat{d}_{\rm out}$ is linear to $\hat{d}$, and the control input vector is $\mathbf{B} = (0, 1, 0)^T$ (superscript T for transpose)—the feedback force is coupled to the mechanical displacement that is linear to $\hat{b}^\dagger$. The system becomes both observable and controllable, as we have $\text{rank}([\mathbf{D};\mathbf{DA};\mathbf{DA}^2]) = \text{rank}([\mathbf{B},\mathbf{AB},\mathbf{A}^2\mathbf{B}]) = 3$. A stabilizing controller can then be constructed (see Sec. 9.4 of Ref. [40]), which has the following transfer function (from $\hat{d}$ to $\hat{b}^\dagger$) in the frequency domain:

$$C(\Omega) = -\mathbf{K}(-i\Omega\mathbf{I} - \mathbf{A} + \mathbf{BK} + \mathbf{LD})^{-1}\mathbf{L}, \tag{21}$$

where $\mathbf{K} = (K_1, K_2, K_3)$ and $\mathbf{L} = (L_1, L_2, L_3)^{\rm T}$ are chosen such that eigenvalues of $\mathbf{A} - \mathbf{LD}$ and $\mathbf{A} - \mathbf{BK}$ all have a negative real part. Given the nominal parameter specification in Eq. (5), the system will be stabilized by setting $\mathbf{K} = 3\times10^5\epsilon^{-1}(-i, 1, -1)$ and $\mathbf{L} = 5\times10^5\epsilon^{-1}(i, 1.2, 1)$, where ϵ is the fraction of the output (in amplitude) measured using heterodyne detection. With this set of $\mathbf{K}$ and $\mathbf{L}$ found, an arbitrary stabilizing controller can be generated via Youla-Kučera parametrization [41], which is used for control optimization.

Rigorous treatment.—We have used several approximations in order to gain intuitive understanding. These

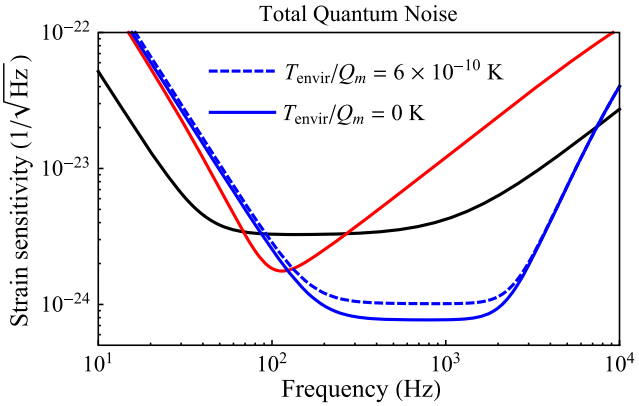

FIG. 6 (color online). The figure shows the total quantum noise (including radiation pressure noise) of the unstable filter scheme at different temperatures. The color code for different curves is the same as in Fig. 2. The test mass is assumed to be 40 kg, the same as for Advanced LIGO.

approximations are reasonable in the parameter regime that we are focusing on. We briefly outline how the more rigorous treatment is applied in the actual analysis for producing the results presented in this Letter. Specifically, the optomechanical interaction in the main interferometer mixes the upper and lower sidebands around ω_0, which was ignored by assuming an infinite test mass and focusing on the shot noise only. The interaction in the optomechanical filter mixes in sidebands around $\omega_0 + 2\omega_m$ that were ignored in the RWA. A rigorous treatment therefore involves propagating four sidebands at frequency $\omega_0 \pm \Omega$ and $\omega_0 + 2\omega_m \pm \Omega$. The result is shown in Fig. 6 as one example. Notice that the low-frequency radiation pressure noise can be reduced by either using a frequency-dependent readout [42] or increasing the test mass size.

Conclusion.—We have proposed the idea of using unstable filters for improving the bandwidth of laser interferometric gravitational-wave detectors. It can also be applied to other quantum measurement devices with resonant cavities, as the underlying principle is the same. The main difficulty for implementing this idea with optomechanics-based filters is the stringent requirement on the thermal noise of the mechanical oscillator, which could be mitigated by using the optical-dilution idea, but requires further experimental verification.

We thank H. Yang, M. Wang, and other members of the LIGO-MQM discussion group for fruitful discussions. H. M. is supported by a Marie-Curie Fellowship. Y. C. is supported by NSF Grant No. PHY-1068881 and NSF CAREER Grant No. PHY-0956189. Y. M. and C. Z. have been supported by the Australian Research Council.

[1] G. M. Harry, Classical Quantum Gravity **27**, 084006 (2010).
[2] The Virgo Collaboration, Classical Quantum Gravity **32**, 024001 (2015).
[3] K. Somiya, Classical Quantum Gravity **29**, 124007 (2012).
[4] J. Mizuno, Ph.D. thesis, University of Hannover, 1995.
[5] M. Aspelmeyer, T. J. Kippenberg, and F. Marquardt, Rev. Mod. Phys. **86**, 1391 (2014).
[6] W. W. Chow, J. Gea-Banacloche, L. M. Pedrotti, V. E. Sanders, W. Schleich, and M. O. Scully, Rev. Mod. Phys. **57**, 61 (1985).
[7] V. B. Braginsky, M. L. Gorodetsky, F. Y. Khalili, and K. S. Thorne, AIP Conf. Proc. **523**, 180 (2000).
[8] M. Tsang, H. M. Wiseman, and C. M. Caves, Phys. Rev. Lett. **106**, 090401 (2011).
[9] C. M. Caves, Phys. Rev. D **23**, 1693 (1981).
[10] K. McKenzie, N. Grosse, W. P. Bowen, S. E. Whitcomb, M. B. Gray, D. E. McClelland, and P. K. Lam, Phys. Rev. Lett. **93**, 161105 (2004).
[11] H. Rehbein, J. Harms, R. Schnabel, and K. Danzmann, Phys. Rev. Lett. **95**, 193001 (2005).
[12] V. Peano, H. G. L. Schwefel, C. Marquardt, and F. Marquardt, arXiv:1502.06423.
[13] The LIGO Scientific Collaboration, Nat. Phys. **7**, 962 (2011).
[14] The LIGO Scientific Collaboration, Nat. Photonics **7**, 613 (2013).
[15] M. Evans, L. Barsotti, P. Kwee, J. Harms, and H. Miao, Phys. Rev. D **88**, 022002 (2013).
[16] H. Miao, H. Yang, R. X. Adhikari, and Y. Chen, Classical Quantum Gravity **31**, 165010 (2014).
[17] The LIGO Scientific Collaboration, Instrument Science White Paper, 2014.
[18] A. Wicht, K. Danzmann, M. Fleischhauer, M. Scully, G. Müller, and R.-H. Rinkleff, Opt. Commun. **134**, 431 (1997).
[19] A. Wicht, M. Müller, R. H. Rinkleff, A. Rocco, and K. Danzmann, Opt. Commun. **179**, 107 (2000).
[20] S. Wise, G. Mueller, D. Reitze, D. B. Tanner, and B. F. Whiting, Classical Quantum Gravity **21**, S1031 (2004).
[21] S. Wise, V. Quetschke, A. J. Deshpande, G. Mueller, D. H. Reitze, D. B. Tanner, B. F. Whiting, Y. Chen, A. Tünnermann, E. Kley *et al.*, Phys. Rev. Lett. **95**, 013901 (2005).
[22] G. S. Pati, M. Salit, K. Salit, and M. S. Shahriar, Phys. Rev. Lett. **99**, 133601 (2007).
[23] H. N. Yum, J. Scheuer, M. Salit, P. R. Hemmer, and M. S. Shahriar, J. Lightwave Technol. **31**, 3865 (2013).
[24] M. Zhou, Z. Zhou, and S. M. Shahriar, Phys. Rev. D **92**, 082002 (2015).
[25] Y. Ma, H. Miao, C. Zhao, and Y. Chen, Phys. Rev. A **92**, 023807 (2015).
[26] A. Buonanno and Y. Chen, Phys. Rev. D **65**, 042001 (2002).
[27] G. I. Harris, D. L. McAuslan, T. M. Stace, A. C. Doherty, and W. P. Bowen, Phys. Rev. Lett. **111**, 103603 (2013).
[28] S. Weis, R. Rivière, S. Deléglise, E. Gavartin, O. Arcizet, A. Schliesser, and T. J. Kippenberg, Science **330**, 1520 (2010).
[29] J. D. Teufel, D. Li, M. S. Allman, K. Cicak, A. J. Sirois, J. D. Whittaker, and R. W. Simmonds, Nature (London) **471**, 204 (2011).
[30] A. H. Safavi-Naeini, T. P. Mayer Alegre, J. Chan, M. Eichenfield, M. Winger, Q. Lin, J. T. Hill, D. E. Chang, and O. Painter, Nature (London) **472**, 69 (2011).
[31] Y. Ma, S. L. Danilishin, C. Zhao, H. Miao, W. Z. Korth, Y. Chen, R. L. Ward, and D. G. Blair, Phys. Rev. Lett. **113**, 151102 (2014).
[32] C. M. Caves, Phys. Rev. D **26**, 1817 (1982).
[33] T. Corbitt, Y. Chen, E. Innerhofer, H. Muller-Ebhardt, D. Ottaway, H. Rehbein, D. Sigg, S. Whitcomb, C. Wipf, and N. Mavalvala, Phys. Rev. Lett. **98**, 150802 (2007).
[34] D. E. Chang, K.-K. Ni, O. Painter, and H. J. Kimble, New J. Phys. **14**, 045002 (2012).
[35] K. K. Ni, R. Norte, D. J. Wilson, J. D. Hood, D. E. Chang, O. Painter, and H. J. Kimble, Phys. Rev. Lett. **108**, 214302 (2012).
[36] W. Z. Korth, H. Miao, T. Corbitt, G. D. Cole, Y. Chen, and R. X. Adhikari, Phys. Rev. A **88**, 033805 (2013).
[37] Y. Chen, J. Phys. B **46**, 104001 (2013).
[38] A. Buonanno and Y. Chen, Phys. Rev. D **67**, 062002 (2003).
[39] A. Buonanno, Y. Chen, and N. Mavalvala, Phys. Rev. D **67**, 122005 (2003).
[40] P. J. Antsaklis and A. N. Michel, *A Linear Systems Primer* (Birkhauser, Boston, 2007).
[41] V. Kucera, in *Proceedings of 21st Mediterranean Conference on Control and Automation, Platanias-Chania, 2013* (IEEE, New York, 2013), p. 776.
[42] H. J. Kimble, Y. Levin, A. B. Matsko, K. S. Thorne, and S. P. Vyatchanin, Phys. Rev. D **65**, 022002 (2001).